ADVANCED MATERIALS

Supporting Information

for *Adv. Mater.,* DOI: 10.1002/adma.202008523

Simultaneously Toughening and Stiffening Elastomers with Octuple Hydrogen Bonding

Yizhi Zhuo, Zhijie Xia, Yuan Qi, Takashi Sumigawa, Jianyang Wu, Petr Šesták, Yinan Lu, Verner Håkonsen, Tong Li, Feng Wang, Wei Chen, Senbo Xiao, Rong Long, Takayuki Kitamura, Liangbin Li, Jianying He, and Zhiliang Zhang**

WILEY-VCH

Supporting Information

Simultaneously toughening and stiffening elastomers with octuple hydrogen bonding

Yizhi Zhuo, Zhijie Xia, Yuan Qi, Takashi Sumigawa, Jianyang Wu, Petr Šesták, Yinan Lu, Verner Håkonsen, Tong Li, Feng Wang, Wei Chen, Senbo Xiao, Rong Long, Takayuki Kitamura, Liangbin Li, Jianying He, and Zhiliang Zhang**

Experimental Section

Synthesis of PDUO and PDUQ

PDUO: Chain extension reaction was used to synthesize PDUO with octuple hydrogen bonding, as shown in Figure S2, Supporting Information. A typical synthesis of PDUO5000 is shown as follows: Aminopropyl terminated polydimethylsiloxane (NH_2-PDMS-NH_2, 75.000 g, 15 mmol, molecular weight: 5000 Dalton, Gelest) was dissolved in tetrahydrofuran (THF, 150 mL, Sigma-Aldrich). Then the solution was dropwise added into isophorone diisocyanate (IDI, 6.6684 g, 30 mmol, Sigma-Aldrich) in THF (45 mL) under vigorous stirring. After stirring for 2 h, 0.5 mL of the mixture was pipetted out and evaporated for characterization (termed as PDUO-m), then 1,2-bis(2-aminoethoxy)ethane (2.223 g, 15 mmol, chain extender, Sigma-Aldrich) in THF (30 mL) was added into the mixture under vigorous stirring. Afterwards, another 20 mL of THF was added into the mixture to lower the viscosity. After stirring for another 48 h, the viscous mixture was stored for further fabrication or testing. PDUO3000 and PDUO1000 followed the same procedure. However, during the synthesis of PDUO1000, precipitation occurred when adding chain extender, leading to the failure of synthesis.

PDUQ3000: IDI (1.1114 g, 5 mmol) in THF (10 mL) was added to NH_2-PDMS-NH_2 (15.000 g, 5 mmol, 50-60 cst, DMS-A15) in THF (45 mL) under vigorous stirring, followed by stirring for another 48 h.

Fabrication of PDUO and PDUQ films for testing

25 mL of the above solution was poured into a homemade Teflon pool mould with a dimension of 7 × 7 × 1 cm^3, covered by petri dish and allowed to dry under ambient conditions for 5 days. Afterwards, the resulting elastomer film was gently peeled off from the mould.

Fabrication of Sylgard 184 films

Sylgard 184 (base : curing agent = 10 : 1) was cured at 65 ºC for 4 hours.

Mechanical testing

The fracture toughness (Γ) of PDUO was characterized by pure shear test that proposed by Rivlin and Thomas[1] which has been widely adopted to characterize fracture of soft materials.[2] The experiments were conducted on a mechanical testing system (Instron 5944 with a 2 kN load cell). A notch of 15 mm in length was made in a rectangular specimen (width: ~60 mm; thickness: ~1 mm), as shown in the inset schematic in Figure S1a, Supporting Information. Specimens with and without notch were fixed in two clamps with a distance of 10 mm, and then subjected to tension with a loading rate of 0.005 mm/mm/s. The fracture toughness (Γ) is given by:[1, 2c]

$$\Gamma = W_c H \quad \text{(S1)}$$

where W_c is the integrating area of the stress-strain curve of the unnotched sample until the critical strain (which is the failure strain of the notched sample), and H is the distance between the two clamps.

Young's modulus (E) of the elastomers was calculated from the slope of fitting of initial stress-strain curves of uniaxial tensile test (Figure S1b, Supporting Information). Specimens (width × thickness: 10 × 1 mm^2) were fixed in two clamps with a distance

of 30 mm, and then subjected to uniaxial tensile testing with a loading rate of 0.015 mm/mm/s.

Fourier transform infrared (FTIR) spectroscopy

FTIR spectra were tested in a FTIR spectrometer (Thermo Nicolet Nexus) equipped with a temperature controller. To study the change of spectra during raising temperature, the spectra after every 10 ºC from 30 ºC to 150 ºC were recorded.

^{1}H nuclear magnetic resonance (NMR) spectroscopy

^{1}H NMR spectra were recorded in a Bruker instrument (Avance III 400 MHz) using the solvent of chloroform-d ($CDCl_3$, Sigma-Aldrich) with tetramethylsilane (TMS) as the internal reference.

Thermogravimetric analysis (TGA)

TGA was conducted by using a Netzsch instrument (TG 209F1 Libra). The sample was placed in the crucible and heated from 30 ºC to 800 ºC with a heating rate of 10 ºC/min under nitrogen atmosphere.

X-ray photoelectron spectroscopy (XPS)

XPS was performed in a Kratos Ultra DLD with 12 mA and 12 kV using a monochromatic Al source. The chamber pressure was 5×10^{-9} mbar. To detect the spectra at different depths, the sample was etched for different times (0, 10, 60, 120, and 180 s) by using an Ar gun at a pressure of 1.5×10^{-6} mbar and 3 kV with raster size of 2×2 mm^2 before measurement. The data were analyzed in the CasaXPS software. All binding energies were referenced to the C 1s peak at 285 eV of the

surface adventitious carbon. Furthermore, the data were background subtracted and smoothed out using a five-point quadratic Savitzky-Golay algorithm.

Modulated differential scanning calorimetry (MDSC)

DSC experiments were carried out by using a Netzsch instrument (DSC 214 Polyma) at a heating ramps of 5 ºC/min, and a modulation amplitude of 0.5 ºC with a period of 60 s.

Atomic force microscopy (AFM)

AFM was conducted in a Veeco Metrology machine (diMultimode V) using PeakForce Quantitative NanoMechanics mode. ScanAsyst-Air probe (Bruker) was used for measurements.

Density Functional Theory (DFT) simulations

The present DFT simulations were performed with the help of ab initio total-energy and molecular-dynamics program VASP (Vienna Ab initio Simulation Package) developed at the Fakultät für Physik, Universität Wien.[3] In the presented study the electron interactions were described with the projector-augmented waves (PAW) potentials as supplied with the VASP code[4] and the exchange correlation energy was evaluated by means of the generalized gradient approximation (GGA) with parametrization of Perdew-Burke-Ernzerhof.[5] The cut off energy was set to 400 eV and the tolerance of the self-consistent cycle to 10^{-6} eV. The meshes for integration over the Brillouin zone were constructed to keep the maximum distance between neighboring k-points along each reciprocal axis smaller than 0.15 $Å^{-1}$. A Gaussian smearing method was adopted with width of 0.1 eV. The relaxation procedures implemented in the VASP code were used to optimized ionic positions before any

tensile/shear tests. The ionic optimization process was applied until the forces between individual ions were relaxed below 10 meV/Å .

The simulation super cells for the DFT calculations were constructed with orthodromic symmetry consisting the a, b and c dimensions that were set to 23, 27 and 11 Å for the small (quadruple HB) and 50, 21 and 11 Å for the large molecules (octuple HB). These cells are depicted in Figure S16, Supporting Information, for unstrained and non-optimized configurations. Both molecules were inserted in the center of the cell and surrounded with vacuum to prevent mutual interactions between the adjacent cells due to the periodic boundary conditions. Before any tensile or shear tests the atomic positions in all simulation cells were optimized according the mentioned criteria.

In the present DFT simulations, we paid our attention to the hydrogen bonds and their strength between both molecules located in individual simulation cells. Here, we must highlight that both molecules were bonded to each other due to these hydrogen connections. These bonds were tested with respect to their strength via the following deformation procedures. The first procedure consisted simple tension, *i.e.* the upper molecule was moved as a rigid block from the bottom one. The movement was realized via the incremental shifts of 0.1 Å . The second deformation was based on the shear test realized via movement of the upper molecule along the *x*-axis. The value of individual shifts (deformation step) was the same as for the first deformation procedure, i.e. 0.1 Å . The bonding force between molecules was determined from the total energy changes with respect to the deformation (shift). Basic principles of these methods are depicted in Figure S17, Supporting Information.

Molecular dynamics (MD) simulations

In the present study, classic MD simulations were performed to reveal the tensile and shear mechanical response of periodic octuple and quadruple HB domains of PDUO and PDUQ at a

molecular level. Note that, for reference, uniaxial tensile mechanical response of HB-domain-free PDMS was also investigated. All the classic MD calculations were carried out using the Large-scale Atomic-Molecular Massively Parallel Simulator (LAMMPS) software package (https://lammps.sandia.gov/). Three-dimensional systems of HB domain and HB domain-free PDMS polymer were investigated by constructing three cells with periodic boundary conditions. The three cells with initial dimensions of 130 × 60 × 60 $Å^3$, 140 × 60 × 60 $Å^3$ and 90 × 60 × 60 $Å^3$ were composed of 36 identical linear PDUQ, PDUO and PDMS polymers with chemical compositions of $C_{98}H_{276}O_{41}N_4Si_{40}$, $C_{116}H_{308}O_{45}N_8Si_{40}$ and $C_{78}H_{234}O_{39}Si_{39}$, respectively. In the simulation cell, all the linear PDUQ, PDUO and PDMS polymers were placed with identical molecular orientation. The consistent valence force field was employed to describe the intra-molecular bond configurations such as bond stretching, angular bending and torsion potentials, and non-bonded interactions between atoms (the 12-6 Lennard-Jones (LJ) and Coulombic potentials) of the two systems.[6] The cutoff parameter of LJ potential was set to be 15 Å. The long-range electrostatic interactions were computed using the particle-particle-particle-mesh (PPPM) method. Prior to the MD calculations, the global configurations of the PDUQ, PDUO and PDMS systems were quasi-statically optimized to a local energetically-favorable system with an energy and force tolerance of 1.0×10^{-4} Kcal/mole and 1.0×10^{-4} Kcal/(mole·Å), respectively. Subsequently, MD simulations of 1000 ps were carried out at zero confining pressure under NPT (constant number of particles, constant pressure, and constant temperature) ensemble for relaxing the systems. The Nosé-Hoover thermostat and barostat methods with damping times of 0.05 and 0.5 ps were applied to control the temperature and pressure, respectively. The velocity-verlet integration with a reasonable timestep of 1 fs was used to integrate the Newton's equations. Then, uniaxial tensile and shear loads were performed on the relaxed samples using the deformation-control technique. A constant tensile/shear strain rate of $5.0 \times 10^8\ s^{-1}$ was applied to deform the

samples. During the deformation, the pressures in the unloading directions were maintained to allow the samples to experience expansion/contraction as a result of the Poisson effect. The atomic stress per atom was computed on the basis of the *virial* definition of stress. The global tensile and shear mechanical stresses were calculated by summing up virial stresses during the deformation.

Small-angle X-ray scattering (SAXS)

In-situ SAXS experiments were conducted in BL16B1 of the Shanghai Synchrotron Radiation Facility (SSRF). The incident X-ray wavelength was λ=0.124 nm and the Pilatus 2M detector was used to collect the 2D SAXS patterns. The distance of the sample from the detector was calibrated to be 1950 mm. The specimen (10 × 35 mm^2) was stretched by a homemade drawing instrument with a Hencky strain rate of 0.005 s^{-1} (Figure S19a, Supporting Information). The time resolution of SAXS was 10 s.

The data was analyzed in the Fit2D software and corrected for background scattering from air and from the sample holder. 1D SAXS integrated curves were obtained from integrating 2D SAXS patterns as a function of

$$q = \frac{4\pi \sin\theta}{\lambda} \tag{S2}$$

where q, θ, and λ are the module of scattering vector, scattering angle and X-ray wavelength respectively. The obtained 1D SAXS curves were fitted the correlation peak with the Lorentz function to get the curves in Figure S19c,d, Supporting Information.[7] The domain distance (d) was calculated from Brag's law,

$$d = \frac{2\pi}{q_{max}} \tag{S3}$$

The domain distances in the transverse direction (d_{TD}) and the stretch direction (d_{SD}) during affine deformations for incompressible materials follow:[7-8]

$$d_{SD} = (\varepsilon + 1) \times d_0 \quad \text{(S4)}$$

$$d_{TD} = (\varepsilon + 1)^{-0.5} \times d_0 \quad \text{(S5)}$$

where ε and d_0 are the engineering strain and domain distance before stretch. Herein, the engineering strain can be easily converted to Hencky strain (ε_H) through the relation:[9]

$$\varepsilon = e^{\varepsilon_H} - 1 \quad \text{(S6)}$$

Therefore, the relationship between domain distances and ε_H during affine deformation can be obtained:

$$d_{SD} = e^{\varepsilon_H} \times d_0 \quad \text{(S7)}$$

$$d_{TD} = (e^{\varepsilon_H})^{-0.5} \times d_0 \quad \text{(S8)}$$

which have been used to plot the solid curves in Figure 4e.

The peak width of 1D SAXS profile is characterized by full-width-at-half-maximum (FWHM), which is calculated from Figure S19c,d, Supporting Information.

Transmittance

Transmittance of samples were measured by a spectrophotometer (Cary 14 UV/Vis/NIR) in the wavelength range of 400 to 800 nm.

***In-situ* scanning electron microscopy (SEM) during stretching**

Elastomer film was cut by using a homemade stamp-type cutter (Figure S20a, Supporting Information) to obtain a dog-bone specimen (gauge section: 3 × 4 mm^2, Figure S20b, Supporting Information). Afterwards, a sharp pre-crack (length: 0.95 mm) was introduced into the gauge section using a craft knife. The tensile test was conducted in a field emission SEM (FE-SEM, Hitachi SU5000). The displacement was applied to the specimen while observing the cracked area.

Supporting Figures

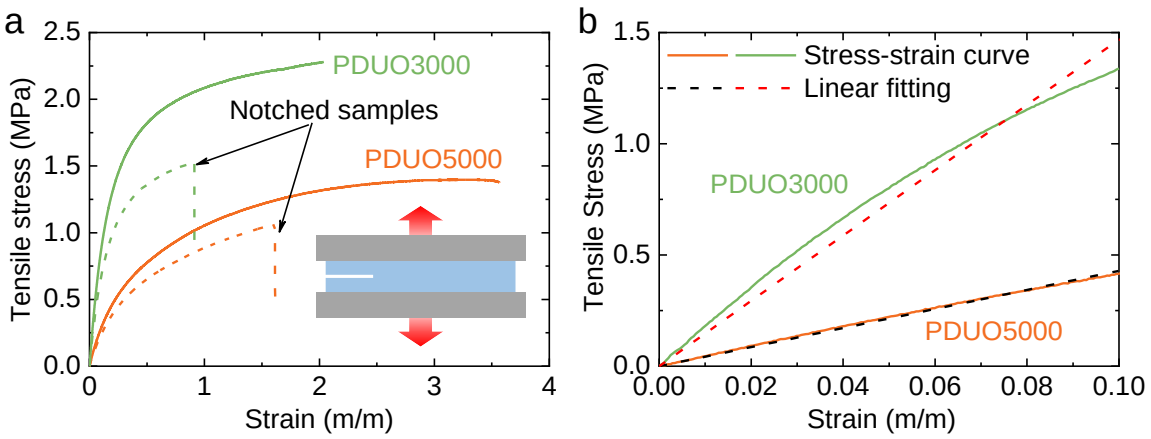

Figure S1. (a) Pure shear test of PDUO. (b) The initial parts of stress-strain curves of uniaxial tensile test of PDUO. The curves are linearly fitted to obtain the slopes corresponding to Young's modulus. The obtained values are reported in Figure 1c in the Main Text.

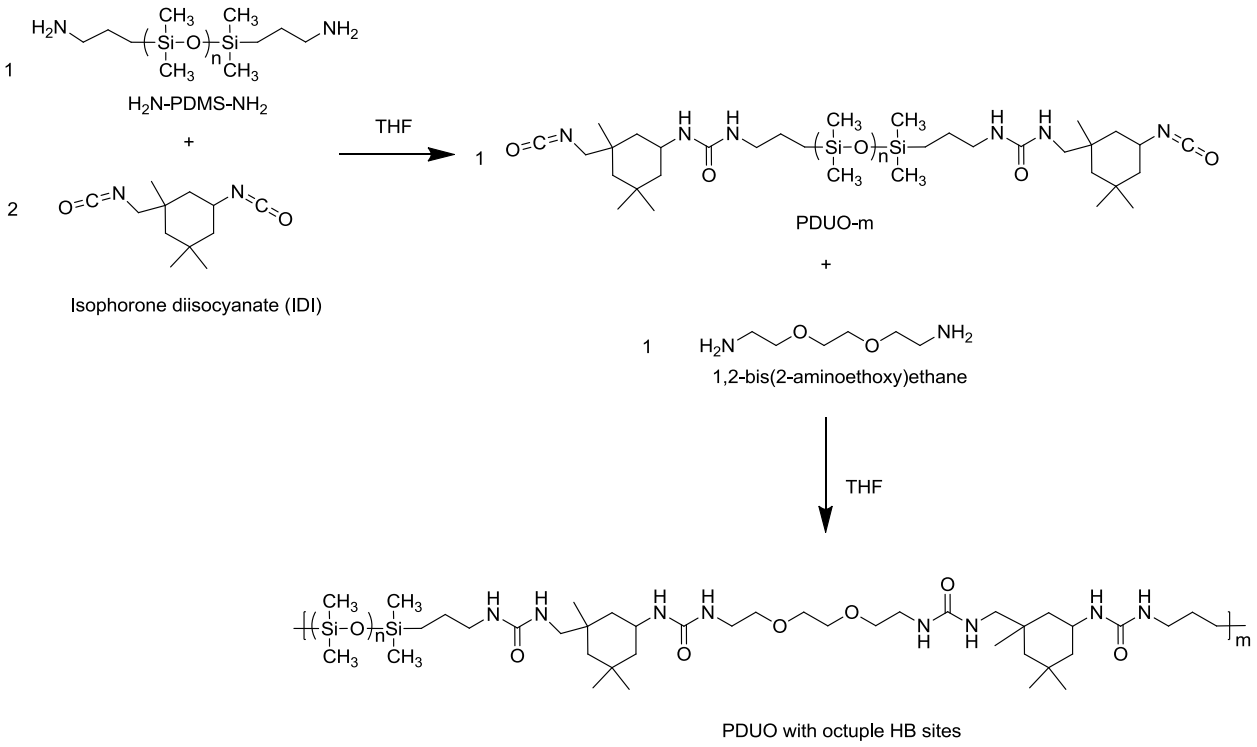

Figure S2. PDUO is synthesized by the chain extension reaction.

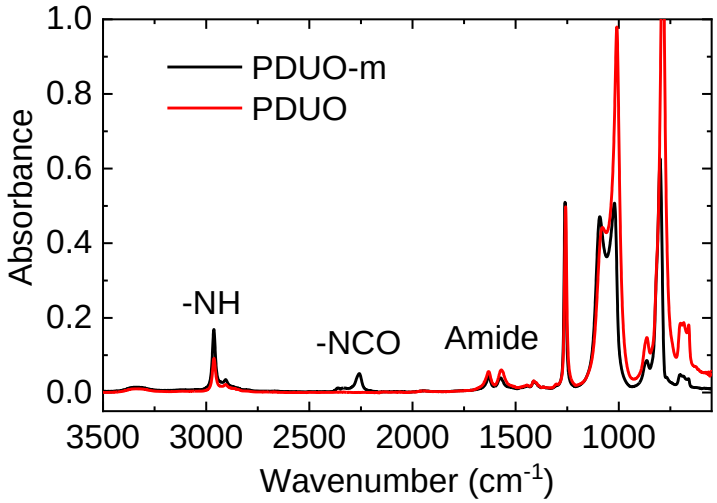

Figure S3. FTIR spectra of PDUO-m and PDUO. Comparing with PDUO-m, the disappearing of peak in PDUO at around 2260 cm^{-1}, which is the characteristic peak of –NCO group, indicates the success of the extension reaction.

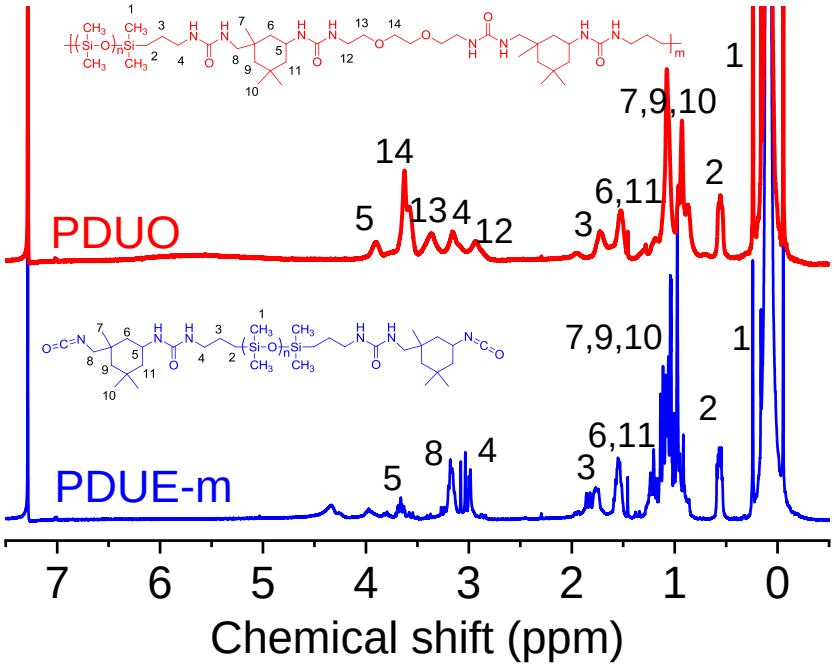

Figure S4. ^{1}H NMR spectra of PDUO-m and PDUO.

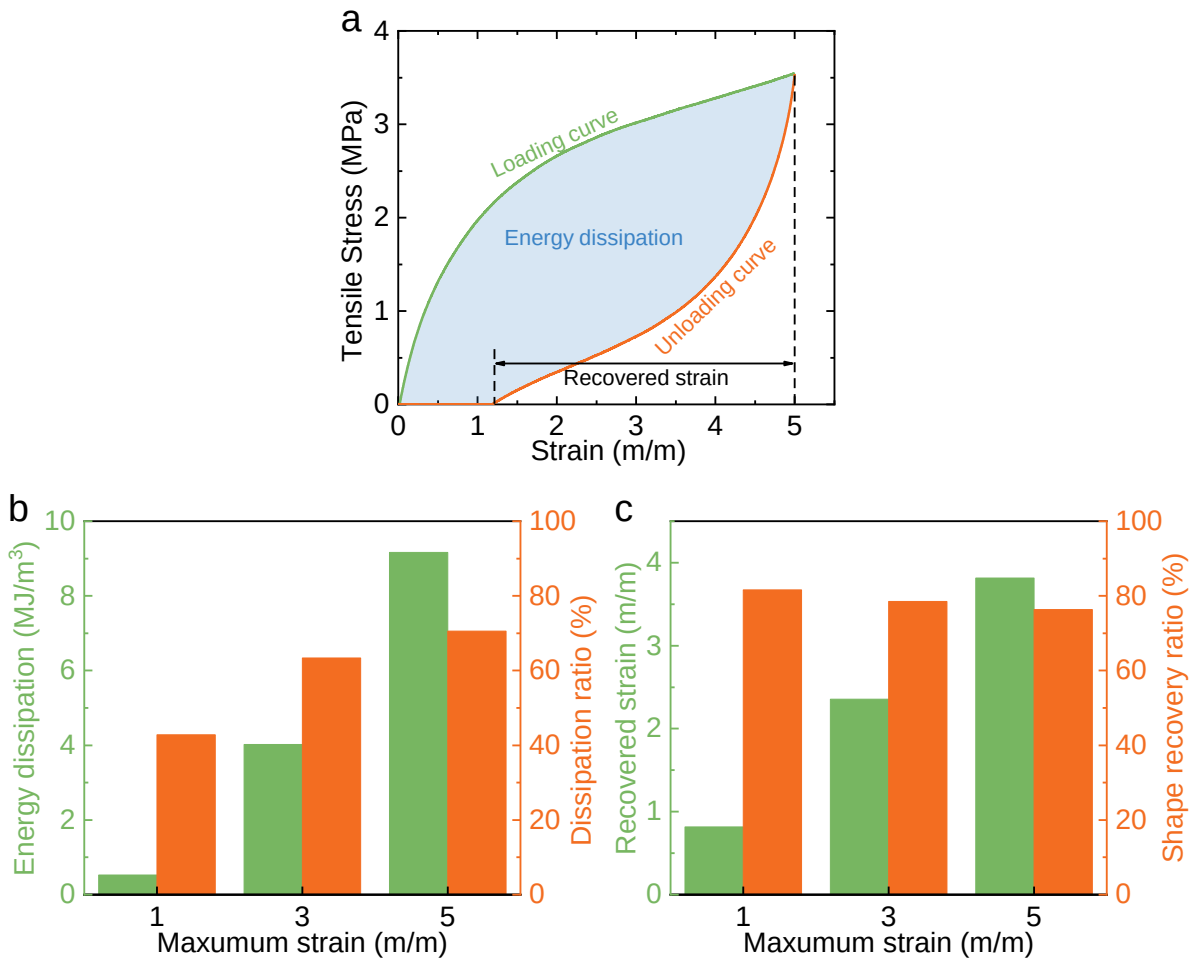

Figure S5. (a) Typical cyclic loading/unloading curves of PDUO. The green line is the loading curve, while orange line is the unloading curve. The light blue area between the loading and unloading curves denotes the energy dissipation. Recovered strain is denoted by the black arrow. (b) Energy dissipations and dissipation ratios at different maximum strains. The dissipation ratio is the ratio between energy dissipation and loading energy (i.e., the area under the loading curve). (c) Recovered strains and shape recovery ratios at different maximum strains. The shape recovery ratio is the ratio between recovered strain and maximum strain.

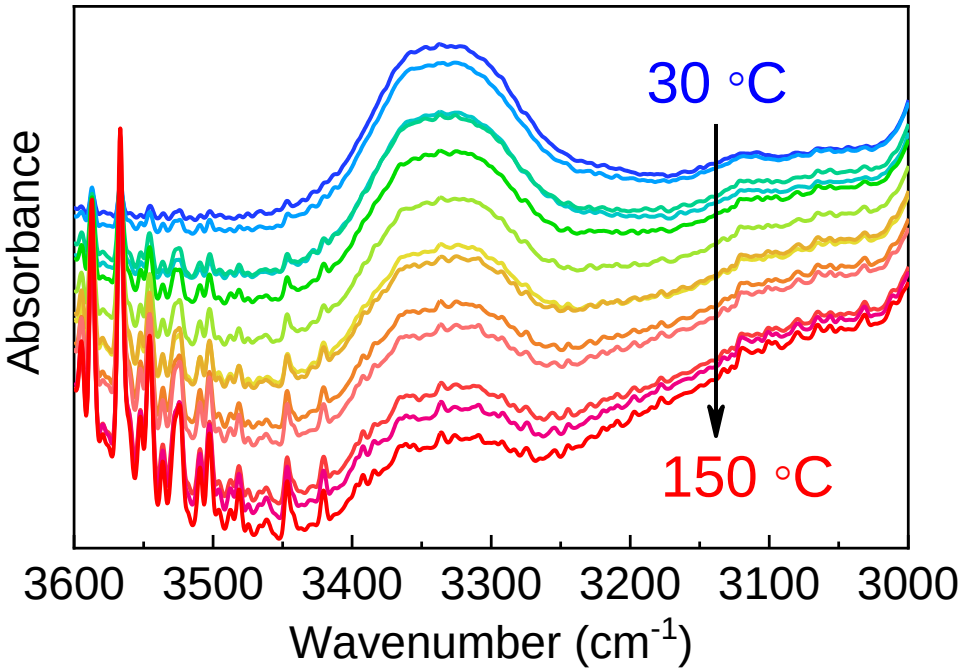

Figure S6. FTIR spectra at an increasing temperature from 30 ºC to 150 ºC in the range of 3600 to 3000 cm^{-1}. In the N-H stretching region (3600~3000 cm^{-1}), the broad bands at ~3330 cm^{-1} correspond to the stretching of hydrogen bonded N-H, decreasing with increasing temperature. At the same time, the peaks at higher frequency, representing the free N-H, arise and increase.

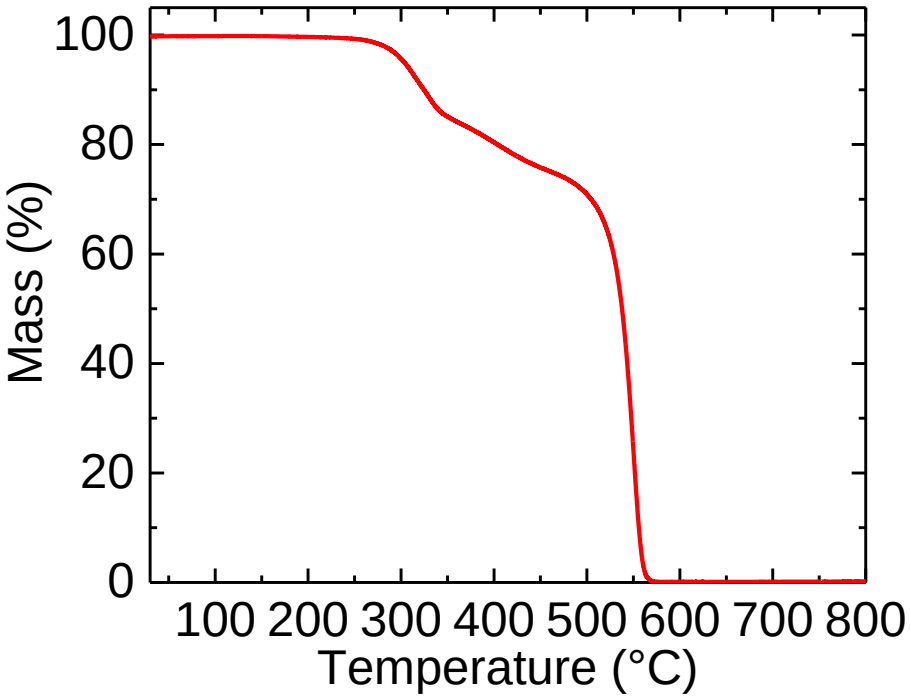

Figure S7. TGA curve of PDUO5000. There is no clear degradation below 250 ºC.

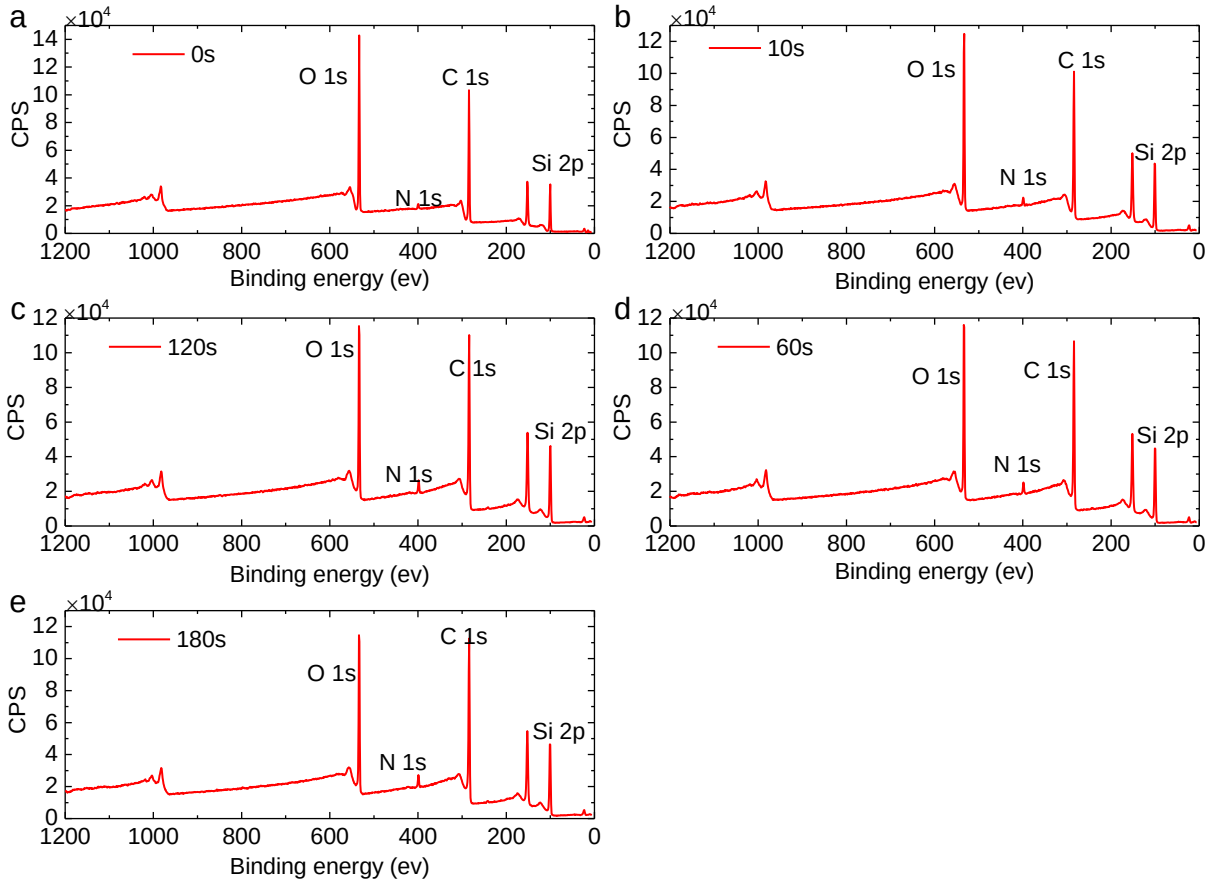

Figure S8. Wide-scan XPS spectra of PDUO5000 after different etching times.

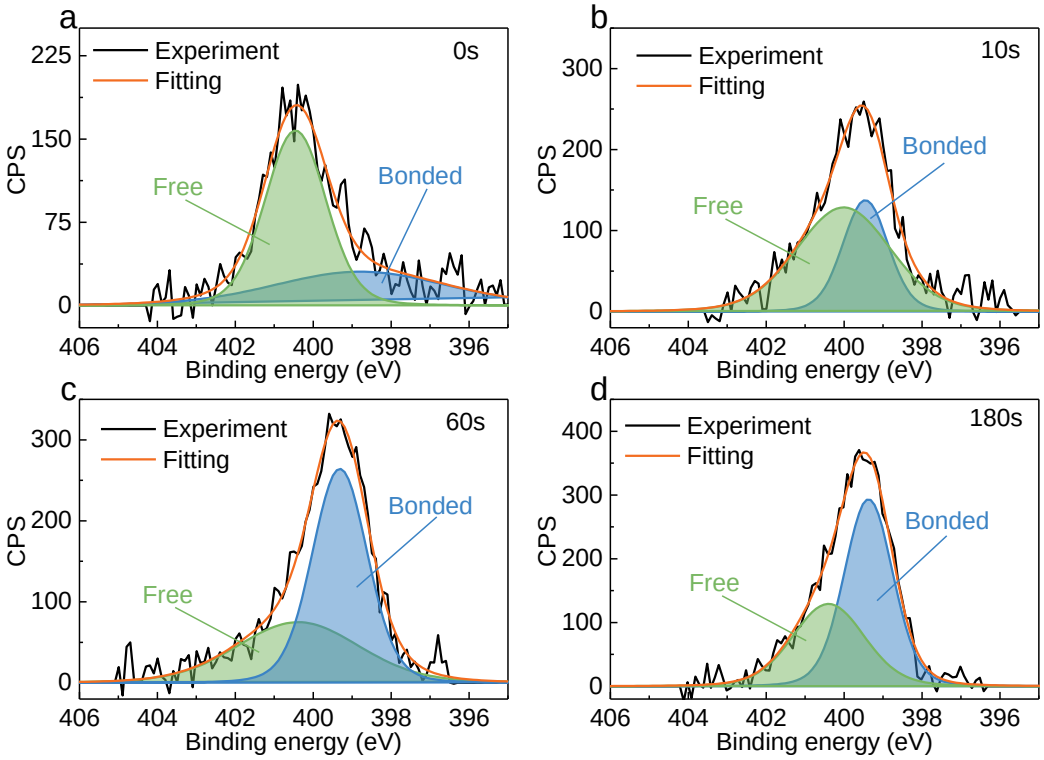

Figure S9. Narrow-scan XPS spectra of PDUO5000 after different etching times

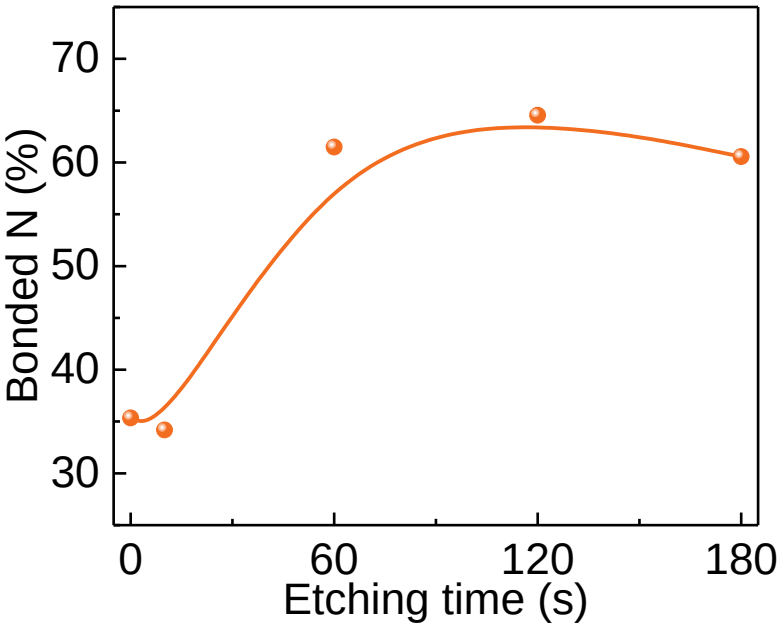

Figure S10. Narrow-scan XPS of PDUO5000 provides the atomic percentage of bonded N as a function of etching time, which is proportional to etching depth.

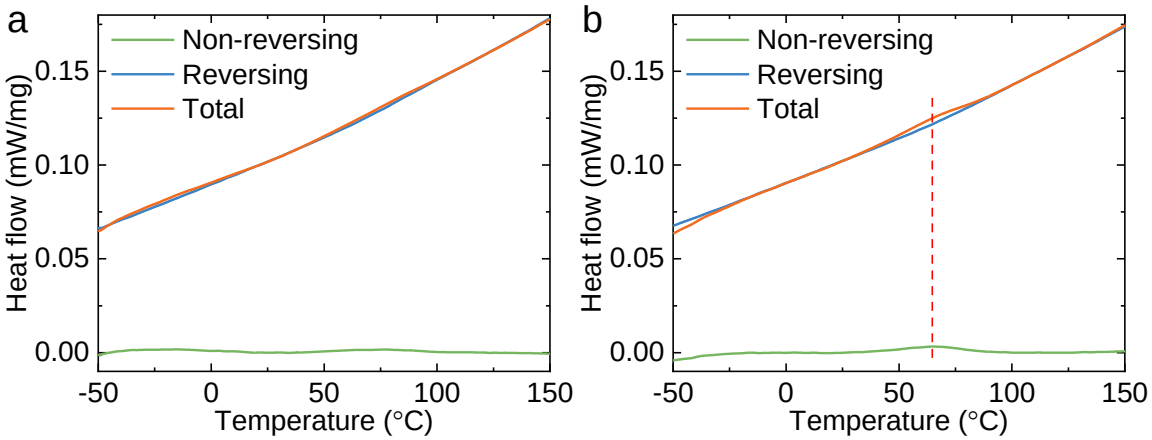

Figure S11. MDSC curves of PDUO. (a) The immediate secondary run. No distinct peak can be observed in all curves. (b) The sample after aging at room temperature for 1 day. An endothermic peak is found at ~65 °C in the non-reversing and total curves, indicating the reformation of HB domains after aging.

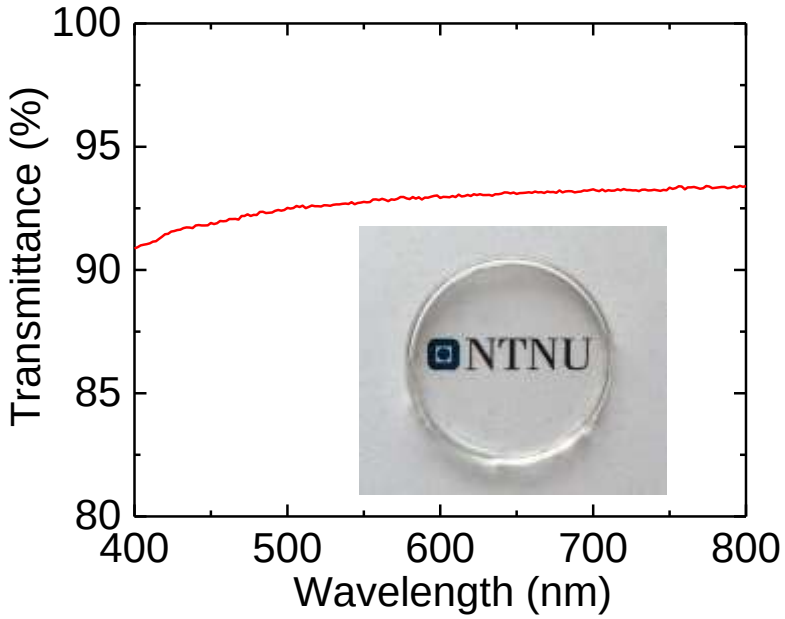

Figure S12. Transmittance of PDUO5000 in the wavelength range of 400 to 800 nm. The inset is a photo of PDUO. The thickness of the PDUO film was measured to be 702 ± 21 μm.

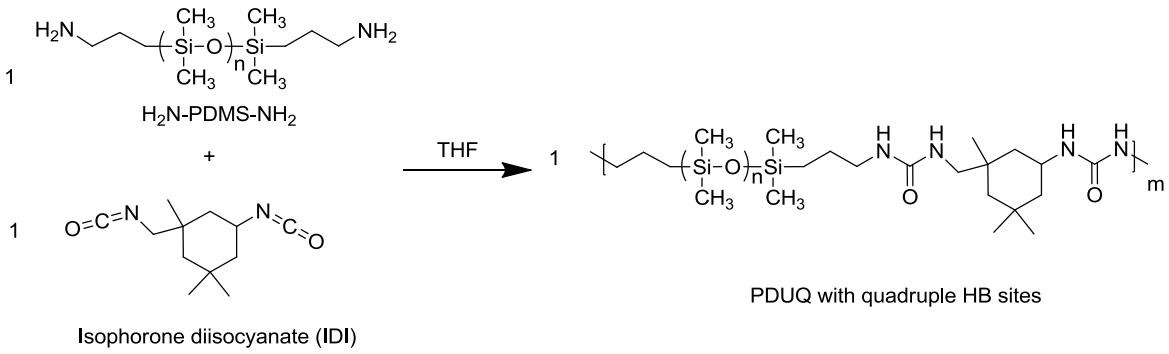

Figure S13. Synthesis of PDUQ.

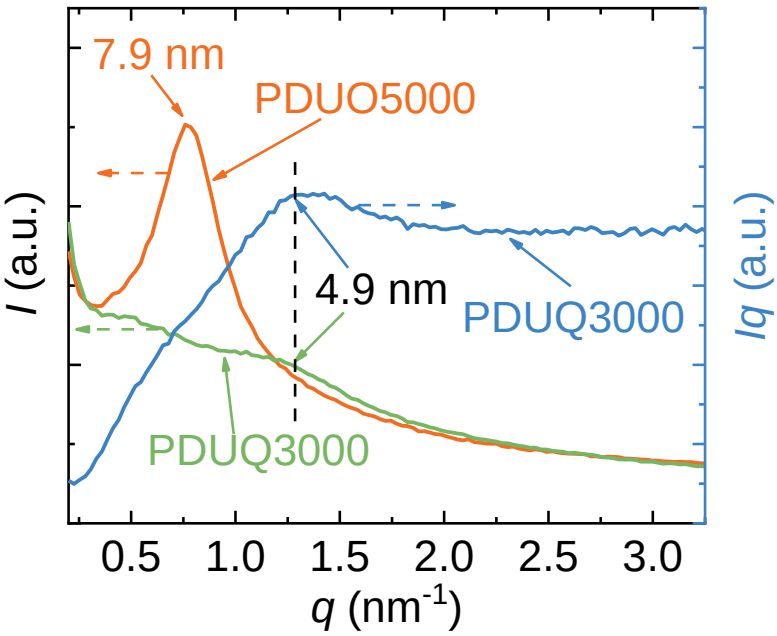

Figure S14. SAXS spectra of PDUO5000 and PDUQ3000. *I*-*q* curves of PDUO5000 and PDUQ3000 are shown in orange and green, respectively. To enhance the visibility of the scattering peak from the *I*-*q* curve of PDUQ3000, we present the *Iq*-*q* curve, which is shown in blue.

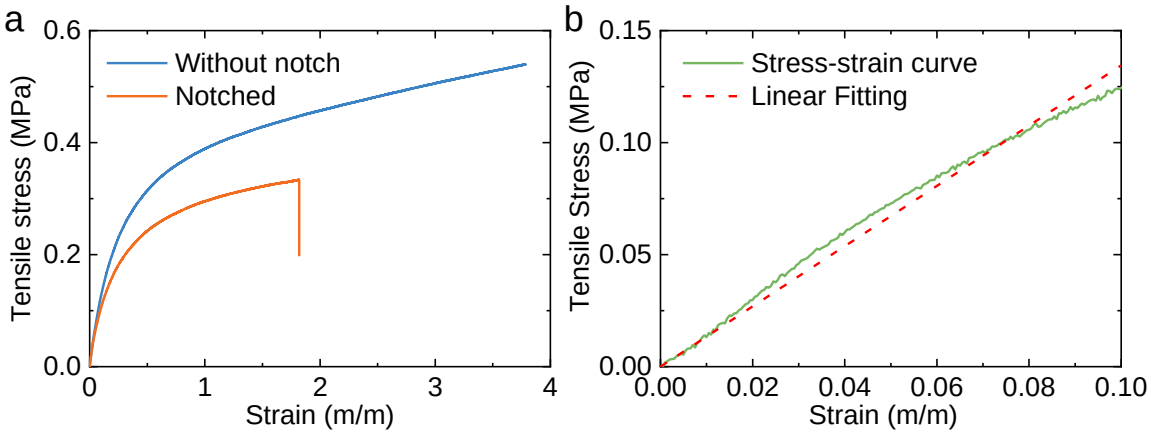

Figure S15. (a) Pure shear test of PDUQ3000. (b) The initial parts of the stress-strain curve of the uniaxial tensile test of PDUQ3000. The curve is linearly fitted to obtain the slope corresponding to Young's modulus.

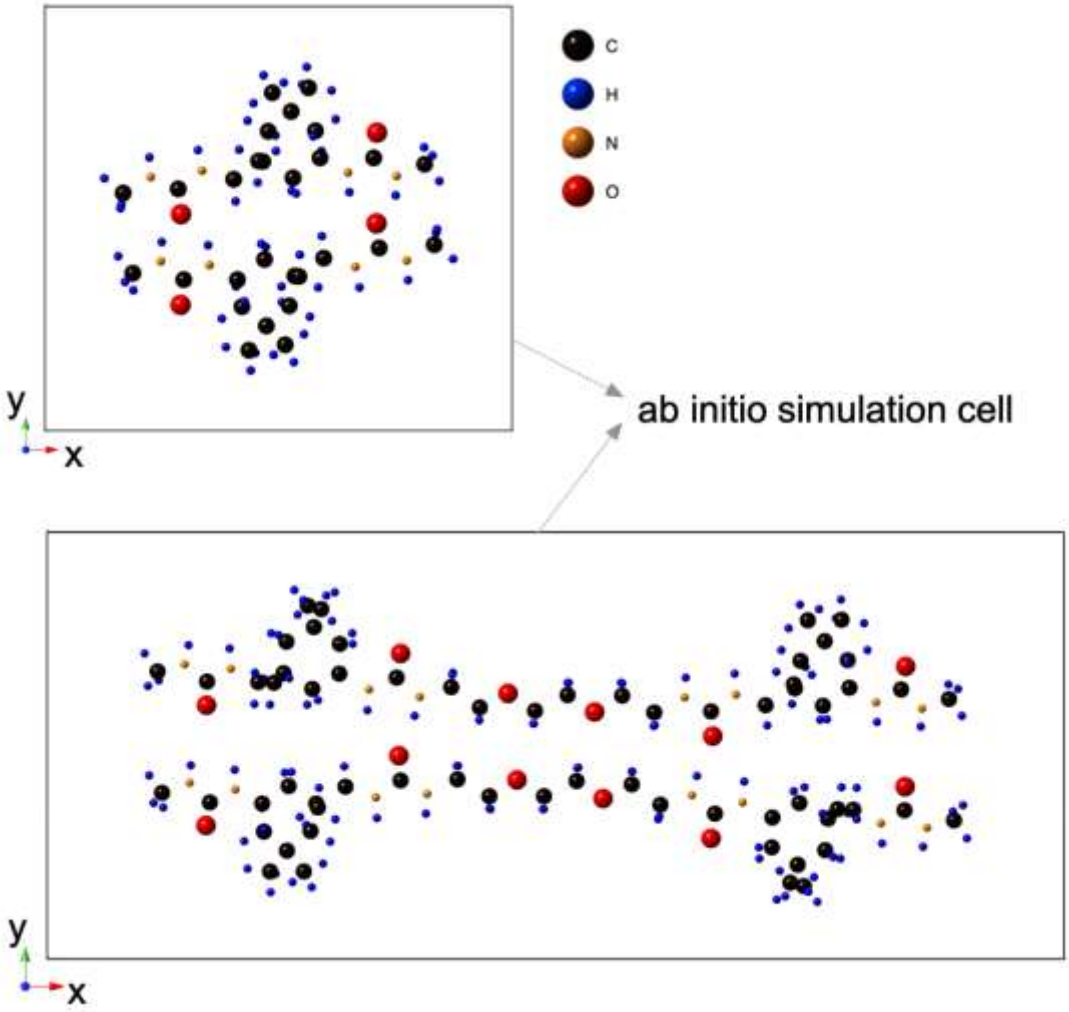

Figure S16. Two types of the simulation cells used in the DFT simulations. The cells comprise a configuration equal to the initial state (before any ionic optimization). The solid black lines represent the size of the simulation cells, i.e. the periodic boundary conditions.

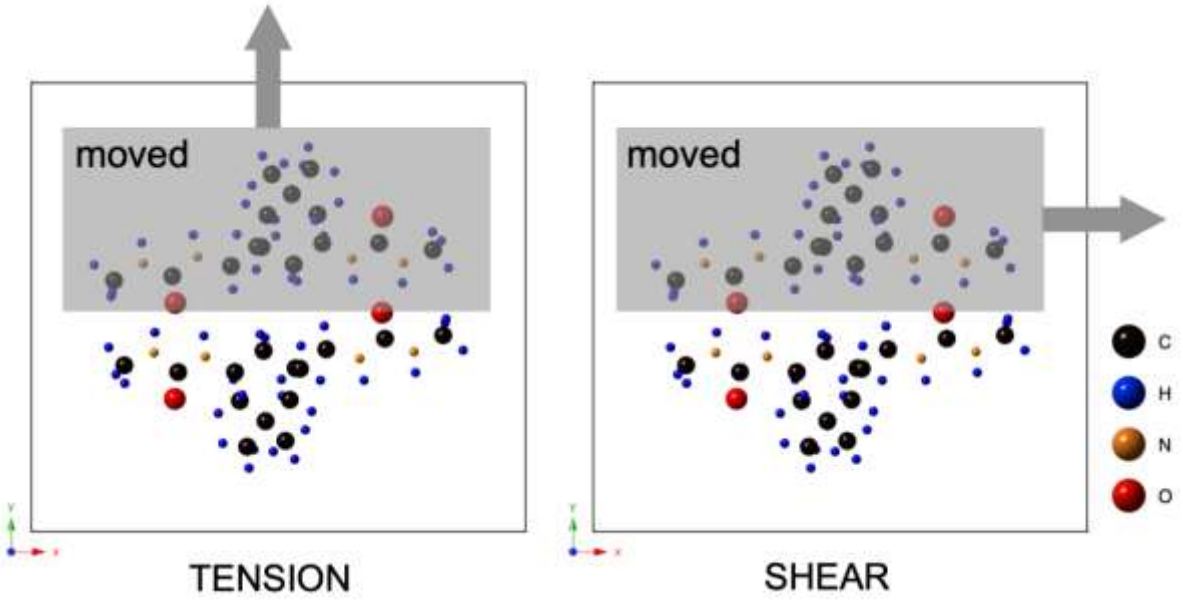

Figure S17. Two deformation modes: the tension (tensile testing) and the shear used in our DFT simulations. The bottom molecule was kept at the fixed position during all simulations while the upper molecule was shifted as a rigid block.

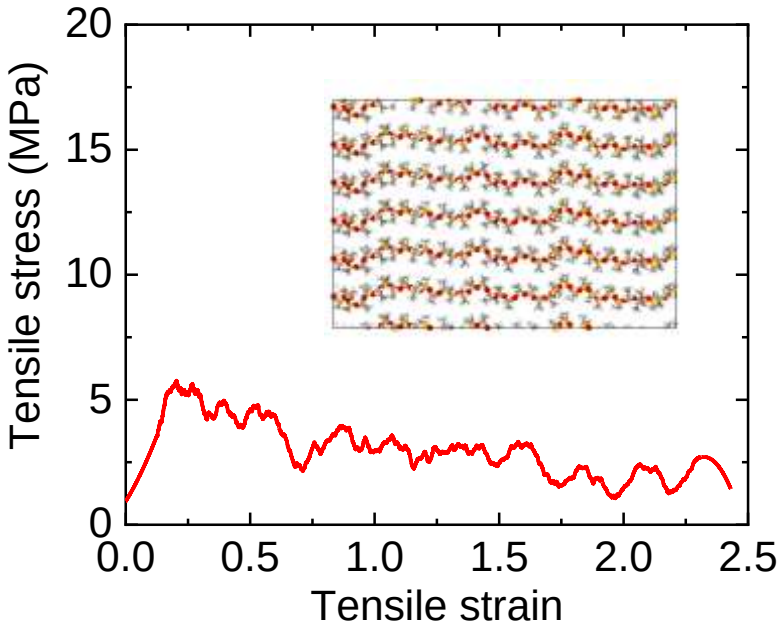

Figure S18. MD tensile stress-strain curves of the PDMS phase. The inset shows the simulation cell of PDMS chains before relaxation.

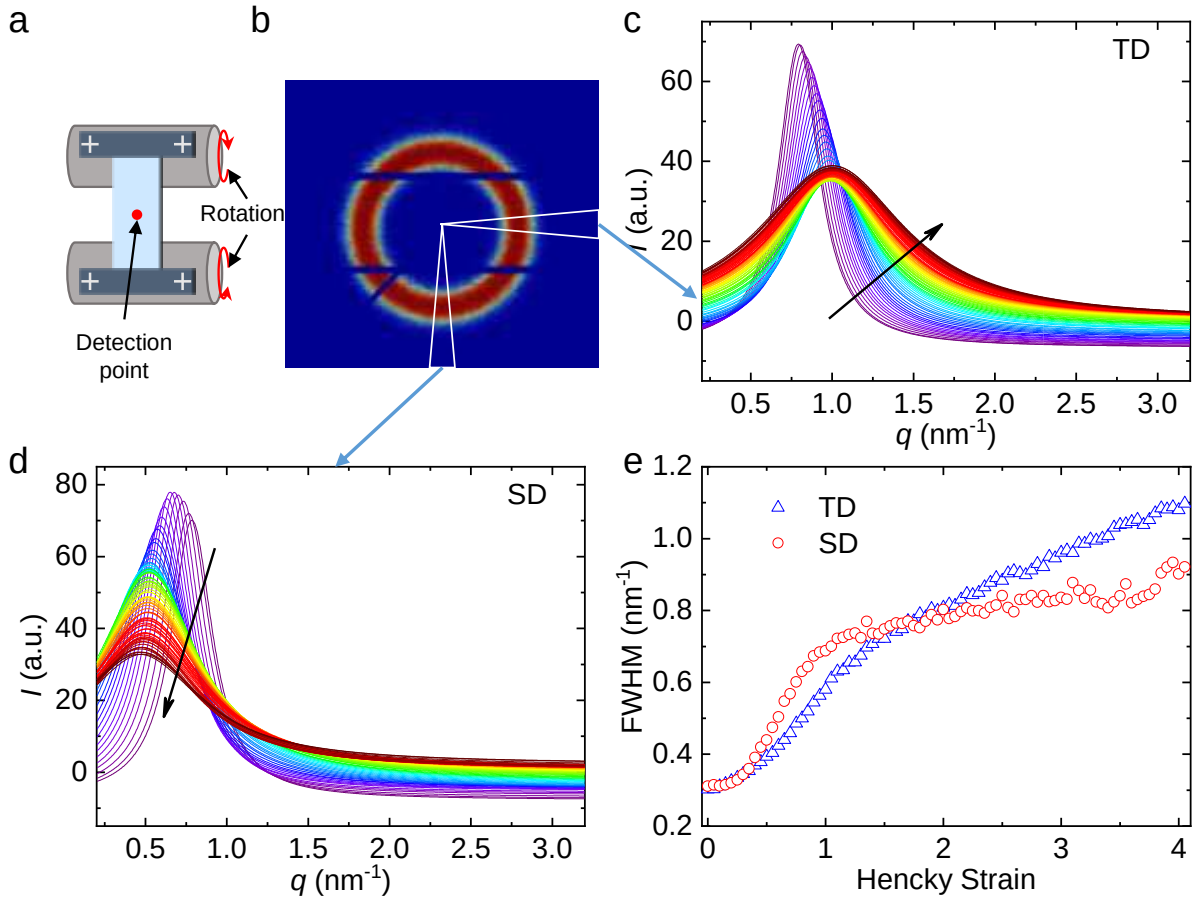

Figure S19. *In-situ* SAXS measurement of PDUO. (a) Schematic of the homemade drawing instrument. (b) The 2D SAXS pattern before stretching, and the integrated areas for obtaining the spectra in the transverse direction (TD) and the stretch direction (SD). (c,d) 1D scattering profiles, intensity (*I*) as a function of *q* at various Hencky strains in the TD and SD, respectively. The black arrows denote the increasing strain. (e) FWHM of 1D scattering profiles as a function of Hencky strain.

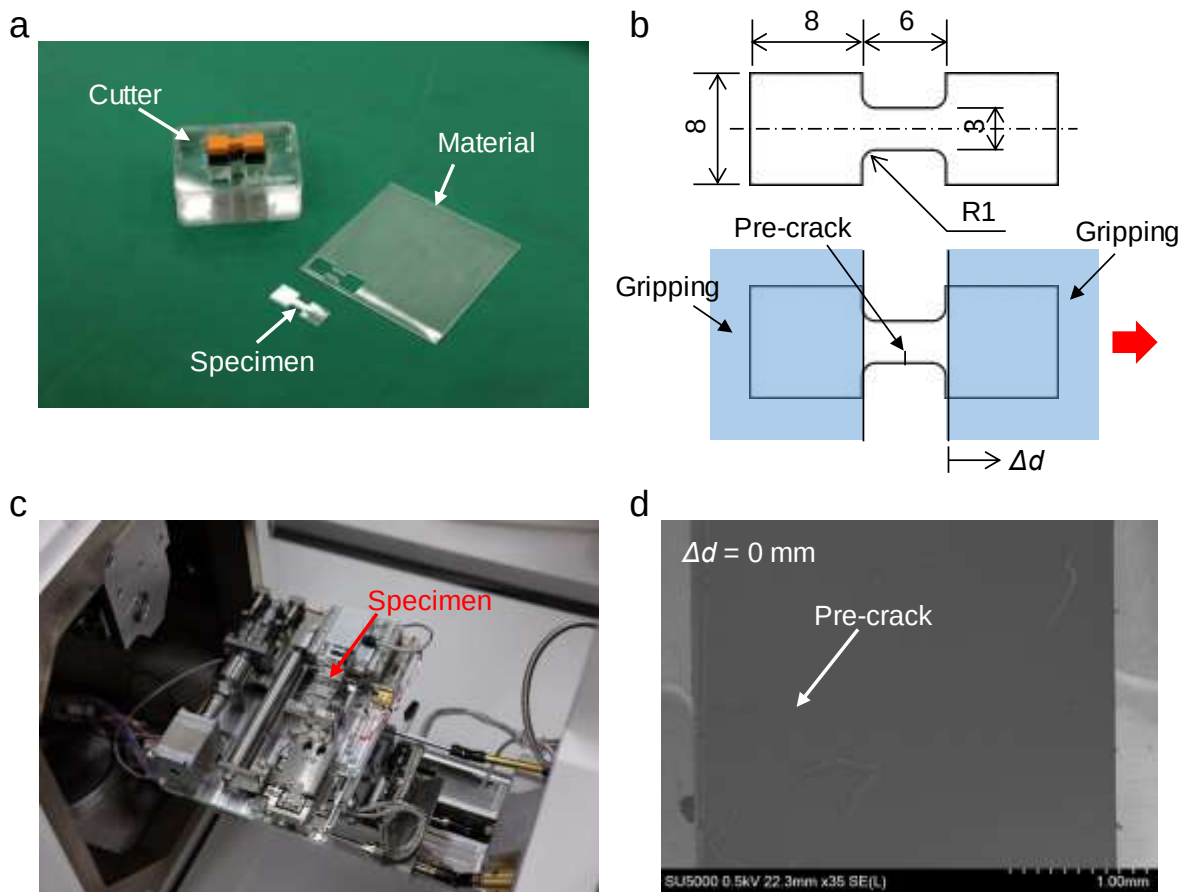

Figure S20. *In-situ* SEM tests. (a) The homemade cutter for the specimen. (b) The dimension of the specimen. (c) The specimen loaded in the test device on the SEM stage. (d) A pre-crack with length of 0.95 mm was introduced in the edge of the specimen.

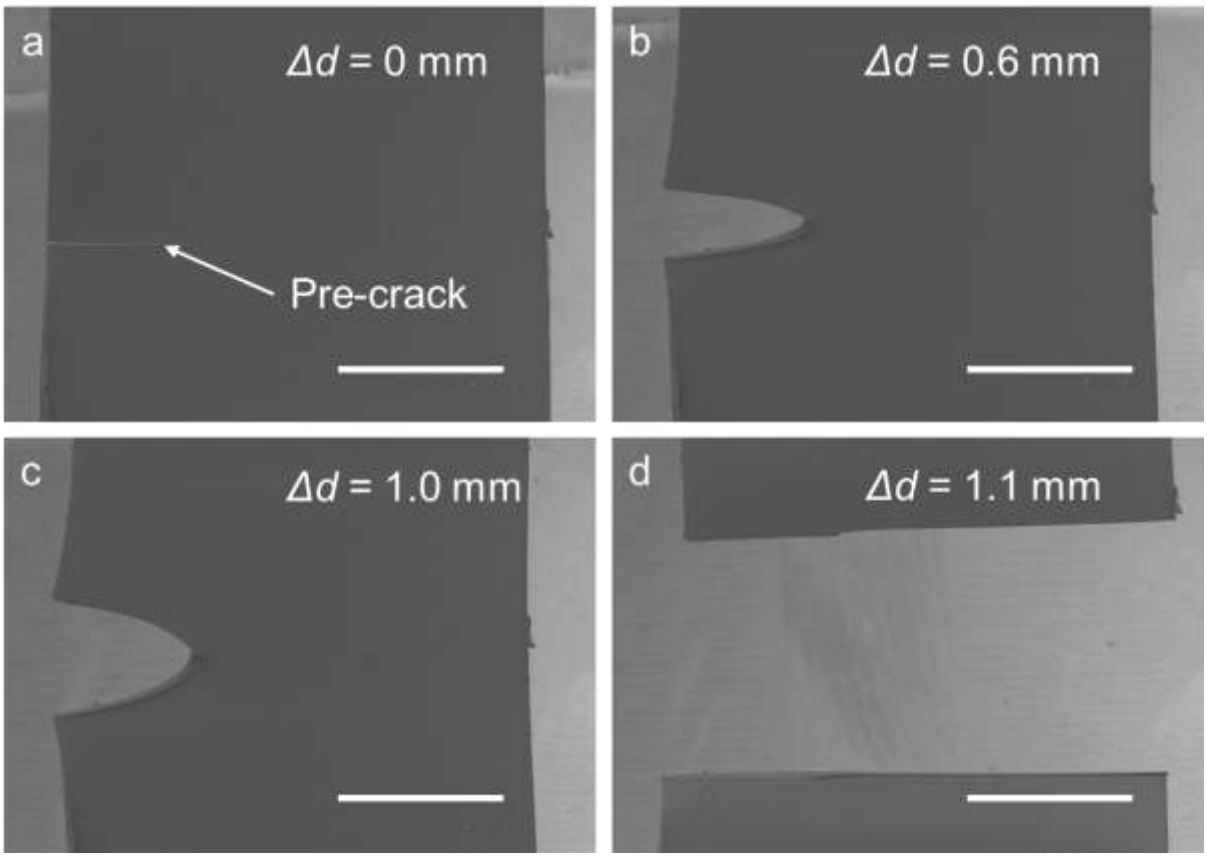

Figure S21. *In-situ* SEM observation of a pre-cracked specimen of Sylgard 184 under tensile test. Gauge length: ~6 mm, as shown in Figure S20. Scale bar: 1.00 mm.

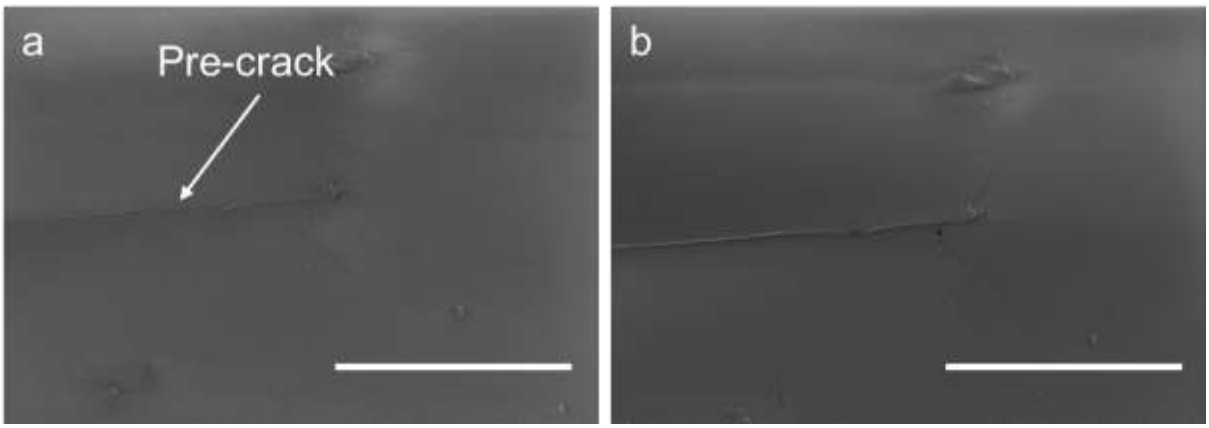

Figure S22. SEM images of the notch tip of a pre-cracked Sylgard 184 film. (a) before and (b) after loading/unloading cycle with a maximum extension of 1.0 mm (before the fracture). Gauge length: ~6 mm, as shown in Figure S20. No clear difference is observed before and after the loading/unloading cycle. Scale bar: 100 μm.

References

[1] R. S. Rivlin, A. G. Thomas, *Journal of Polymer Science* **1953**, 10, 291.
[2] a) J. Y. Sun, X. Zhao, W. R. Illeperuma, O. Chaudhuri, K. H. Oh, D. J. Mooney, J. J. Vlassak, Z. Suo, *Nature* **2012**, 489, 133; b) Y. Qi, J. Caillard, R. Long, *Journal of the Mechanics and Physics of Solids* **2018**, 118, 341; c) R. Long, C. Y. Hui, *Soft Matter* **2016**, 12, 8069.
[3] G. Kresse, J. Furthmuller, *Phys Rev B Condens Matter* **1996**, 54, 11169.
[4] G. Kresse, D. Joubert, *Physical Review B* **1999**, 59, 1758.
[5] J. P. Perdew, K. Burke, M. Ernzerhof, *Phys Rev Lett* **1996**, 77, 3865.
[6] P. Dauber-Osguthorpe, V. A. Roberts, D. J. Osguthorpe, J. Wolff, M. Genest, A. T. Hagler, *Proteins* **1988**, 4, 31.
[7] K. Cui, T. L. Sun, X. Liang, K. Nakajima, Y. N. Ye, L. Chen, T. Kurokawa, J. P. Gong, *Phys Rev Lett* **2018**, 121, 185501.
[8] Q. Wen, A. Basu, P. A. Janmey, A. G. Yodh, *Soft Matter* **2012**, 8, 8039.
[9] C. M. Roland, J. N. Twigg, Y. Vu, P. H. Mott, *Polymer* **2007**, 48, 574.